



Tannic acid, a novel histone acetyltransferase inhibitor, prevents non-alcoholic fatty liver disease both in vivo and in vitro model

Min-Yu Chung¹, Ji-Hye Song², Jinhyuk Lee^{3,4}, Eun Ju Shin^{1,5}, Jae Ho Park¹, Seung-Hyun Lee⁶, Jin-Taek Hwang^{1,5,**}, Hyo-Kyoung Choi^{1,*}

ABSTRACT

Objective: We examined the potential of tannic acid (TA) as a novel histone acetyltransferase inhibitor (HATI) and demonstrated that TA prevents non-alcoholic fatty liver disease (NAFLD) by inhibiting HAT activity.

Methods: The anti-HAT activity of TA was examined using HAT activity assays. An in vitro NAFLD model was generated by treating HepG2 cells with oleic and palmitic acids. Male C57BL/6J mice were fed a control diet (CD) or Western diet (WD) with or without supplementation with either 1% or 3% TA (w/w) for 12 weeks. Finally, the possibility of interacting p300 and TA was simulated.

Results: TA suppressed HAT activity both in vitro and in vivo. Interestingly, TA abrogated occupancy of p300 on the sterol regulatory element in the fatty acid synthase and ATP-citrate lyase promoters, eventually inducing hypoacetylation of H3K9 and H3K36. Furthermore, TA decreased acetylation at lysine residues 9 and 36 of histone H3 protein and that of total proteins. Consequently, TA decreased the mRNA expression of lipogenesis-related genes and attenuated lipid accumulation in vivo. We observed that NAFLD features, including body weight, liver mass, fat mass, and lipid profile in serum, were improved by TA supplementation in vivo. Finally, we demonstrated the possibility that TA directly binds to p300 through docking simulation between ligand and protein.

Conclusions: Our findings demonstrate that TA, a novel HATI, has potential application for the prevention of NAFLD.

© 2018 The Authors. Published by Elsevier GmbH. This is an open access article under the CC BY-NC-ND license (<http://creativecommons.org/licenses/by-nc-nd/4.0/>).

Keywords Histone acetyltransferase; Histone deacetylase; Lipogenesis; Non-alcoholic fatty liver disease; Tannic acid

1. INTRODUCTION

Non-alcoholic fatty liver disease (NAFLD) covers a wide spectrum of various liver diseases [1]. The clinical burden of NAFLD is not only limited to liver-related morbidity and mortality but also involves several extrahepatic dysfunctions, indicating that NAFLD is a multisystem disease [2,3]. Currently, no effective treatment is available for NAFLD. To develop efficacious preventive and therapeutic options, researchers have investigated the cellular and molecular mechanisms, particularly genetic factors, underlying the development of NAFLD. Although genetic factors contribute to the development of NAFLD, environmental factors, including diet and exercise, which have an influence on epigenetic factors, are also key determinants [4,5]. The environment regulates the expression of genes involved in carbohydrate and lipid metabolism by altering histone acetylation patterns

in the chromatin [6]. Histone acetylation is a representative epigenetic mechanism, which is regulated by histone acetyltransferases (HATs) and deacetylases (HDACs). An imbalance between HAT and HDAC activities is associated with various human diseases, including cancer, inflammation, and metabolic disorders [7]. Although many small molecules that modulate HDAC activity have been extensively studied [8], little information is available regarding the modulation of HAT activity, even though HAT enzymes are involved in the onset of various diseases.

In NAFLD models, the “first hit” is liver fat accumulation, which causes insulin resistance, whereas the interplay of inflammatory cytokines, which causes inflammation, acts as the representative “second hit” [9]. However, recently, the “multiple hit” hypothesis has taken into consideration that multiple insults, including insulin resistance, nutritional factors, gut microbiota, and genetic and epigenetic factors, act

¹Korea Food Research Institute, Jeollabuk-do 55365, Republic of Korea ²Department of Biomedical Sciences, Asan Medical Center, University of Ulsan College of Medicine, Seoul 05505, Republic of Korea ³Korea Research Institute of Bioscience and Biotechnology, Daejeon 34141, Republic of Korea ⁴Department of Bioinformatics, Korea University of Science and Technology, Daejeon 34113, Republic of Korea ⁵Department of Food Biotechnology, Korea University of Science & Technology, Daejeon 34113, Republic of Korea ⁶Department of Biochemistry and Molecular Biology, Yonsei University College of Medicine, 03722 Seoul, Republic of Korea

*Corresponding author. Fax: +82 63 219 9876. E-mail: chkyoung@kfri.re.kr (H.-K. Choi).

**Corresponding author. Korea Food Research Institute, Jeollabuk-do, Republic of Korea. Fax: +82 63 219 9876. E-mail: jthwang@kfri.re.kr (J.-T. Hwang).

Received September 21, 2018 • Revision received October 31, 2018 • Accepted November 2, 2018 • Available online 10 November 2018

<https://doi.org/10.1016/j.molmet.2018.11.001>

Abbreviations

ACLY	ATP-citrate lyase	LDL-C	LDL cholesterol
CBP	CREB-binding protein	H&E	hematoxylin and eosin
CD	control diet	NAFLD	non-alcoholic fatty liver disease
ChIP	chromatin immunoprecipitation	NE	nuclear extract
ChREBP	carbohydrate-responsive element-binding protein	OPA	oleic and palmitic acids
DGAT2	diacylglycerol acyltransferase 2	PPAR γ	peroxisome proliferator-activated receptor gamma
EGCG	epigallocatechin-3-gallate	qRT-PCR	quantitative real-time RT-PCR
FASN	fatty acid synthase	SRE	sterol regulatory element
PCAF	p300/CBP-associated factor	SREBP-1c	sterol regulatory element-binding protein 1c
HAT	histone acetyltransferase	TA	tannic acid
HATi	histone acetyltransferase inhibitor	TG	triglyceride
HDAC	histone deacetylase	WD	Western diet
		WST-1	water-soluble tetrazolium salt

collectively to induce NAFLD and provides a more accurate explanation of NAFLD pathogenesis [10]. The p300 HAT enzyme, which functions as a transcriptional coactivator, is co-recruited with nuclear factor- κ B to regulate various inflammatory signaling pathways [11]. Carbohydrate-responsive element-binding protein (ChREBP) is a transcriptional activator of lipogenic genes, which plays a major role in the development of NAFLD [12]. p300 increases ChREBP transcriptional activity through acetylation of Lys-672, which, in turn, increases p300 occupancy on target gene promoters [13]. Furthermore, p300 overexpression results in NAFLD, insulin resistance, and inflammation [13]. However, little is known regarding the role of HATs in the development of NAFLD.

During an ongoing screening study using an *in vitro* HAT assay system to identify phytochemical compounds with HAT inhibitory activity, we identified tannic acid (TA) as a novel HAT inhibitor (HATi) with specificity for major HAT enzymes. TA, a plant-derived hydrolysable tannin polyphenol, is a gallic acid polymer glucoside found in many dietary plant products such as coffee, tea, cocoa, and sorghum grain [14]. Various studies have revealed the beneficial effects of TA [15–17]. Recent studies have shown the anti-obesity effects of TA [18,19]; however, no explanation has been provided regarding the exact molecular mechanism of TA activity on signaling pathways. Furthermore, no study has shown beneficial effects of TA on the development of NAFLD, even though this disease is closely associated with components of the metabolic syndrome, such as obesity, insulin resistance, and dyslipidemia [20].

In the present study, we investigated the potential of TA as a novel HATi and demonstrated that TA prevented the development of NAFLD via its HATi activity, both *in vitro* and *in vivo*.

2. MATERIALS AND METHODS

2.1. Cell culture

HepG2 cells were purchased from the American Type Culture Collection (Manassas, VA, USA). Cells were cultured in a humidified atmosphere of 5% CO₂ at 37 °C in high-glucose DMEM supplemented with 10% fetal bovine serum and antibiotics (Welgene, Daegu, Korea). To establish a NAFLD model using HepG2 cells, we used a non-fat BSA-conjugated combination of oleic acid (Sigma–Aldrich, St. Louis, MO, USA) and palmitic acid (Sigma) at a ratio of 4:1 (OPA). To evaluate the effect of TA on hepatic lipid accumulation, HepG2 cells were concurrently treated with TA and OPA at the indicated concentrations for 18 h. Epigallocatechin-3-gallate (EGCG) was used under the same conditions.

2.2. Cytotoxicity

HepG2 cells were seeded in 24-well plates at 5×10^4 cells/well and, after reaching approximately 70% confluence, were treated with TA at 10, 25, 50, or 100 μ M, in the presence or absence of OPA. After a 24-h incubation, the cells were treated with 10 μ L of a water-soluble tetrazolium salt (WST-1) solution (Enzo Life Sciences, Inc., Farmingdale, NY, USA) for 3 h. Thereafter, 100 μ L of the supernatant was transferred to a 96-well plate, and the absorbance was measured at 450 nm (Molecular Devices, Sunnyvale, CA, USA).

2.3. Lipid content

HepG2 cells were seeded in 24-well plates at 5×10^4 cells/well. After reaching approximately 70% confluence, they were treated in the presence or absence of OPA, with TA at 10 or 25 μ M. After a 24-h incubation, the cells were washed with 200 μ L of PBS, and fixed with 200 μ L of 4% paraformaldehyde for 15 min at room temperature. The cells were then washed three times with PBS and incubated with 200 μ L of 60% isopropanol for 5 min, followed by staining with 200 μ L of 0.1% Oil red O staining solution (Sigma–Aldrich) for 1 h. After additional washing with water, images were captured under a light microscope (Olympus IX51; Olympus Corporation, Central Valley, PA, USA). For lipid quantification, isopropanol was added to each well to dissolve the lipid-stained red dye. After 10 min, the absorbance was measured at 510 nm (Molecular Devices).

2.4. Histone extraction

Cells were seeded at a concentration of 5×10^6 in 10-mm dishes. When cells had reached approximately 70% confluence ($\sim 2 \times 10^8$ cells), they were treated with OPA with or without TA at the indicated concentrations for 18 h. HepG2 cells were lysed according to the manufacturer's protocol (Abcam, Cambridge, MA, USA). The cells were washed with PBS and lysed with pre-lysis buffer to isolate the nuclear fraction. The nuclear pellet was resuspended in lysis buffer, incubated for 30 min on ice, and centrifuged at 10,000 rpm for 5 min at 4 °C. The supernatant was transferred to a clean tube, to which DTT buffer was added. Samples were stored at -70 °C until analysis.

2.5. *In vitro* HAT and HDAC assays

HeLa cell nuclear extract was purchased from BioVision Biotechnology (Milpitas, CA, USA). HAT and HDAC activities in the nuclear extracts were assessed using a commercially available kit according to the manufacturer's protocol (BioVision Biotechnology). To examine the inhibitory effect of TA on specific HATs, we used 100 ng of CREB-binding protein (CBP), p300, or p300/CBP-associated factor (pCAF)

recombinant enzyme as the enzyme source instead of the nuclear extracts. IC50 values were calculated using Prism 5 software (Version 5.03; GraphPad Software Inc., CA, USA). For autoradiography-based in vitro HAT activity assays, HeLa cell nuclear extract was incubated with HAT assay buffer (50 mM HEPES, pH 8.0; 10% glycerol; 1 mM DTT; 1 mM phenylmethylsulfonyl fluoride; and 10 mM sodium butyrate), 1 μ L [3 H] acetyl-CoA, and 5 μ g of biotinylated-H4 peptide (Millipore, Billerica, MA, USA) along with TA at the indicated concentrations at 30 °C for 1 h. The reactions were stopped by adding 5 \times sodium dodecyl sulfate-polyacrylamide gel electrophoresis (SDS-PAGE) sample buffer and samples were separated on 15% SDS-PAGE gels, followed by autoradiographic analysis.

2.6. Quantitative real-time RT-PCR

Cells were seeded in 24-well plates at 5×10^4 cells/well. After reaching approximately 70% confluence, they were treated in the presence or absence of OPA, with TA at indicated concentrations. After an 18-h incubation, total RNA was isolated using TRIzol reagent (Invitrogen, Carlsbad, CA, USA). qRT-PCR was performed using an I Cycler iQ system (Bio-Rad, Hercules, CA, USA) using SYBR Green PCR master mix (Thermo Fisher Scientific, Waltham, MA, USA). PCR amplification was carried out in triplicate using the primers listed in Supplemental Table 1. mRNA levels were normalized to those of glyceraldehyde-3-phosphate dehydrogenase (*GAPDH*) mRNA, and relative expression levels were calculated using the comparative $\Delta\Delta$ CT method [21].

2.7. Immunoblotting

Following cell treatment under the same conditions as used for qRT-PCR, cells were washed with cold PBS and collected. Cell extracts were prepared using RIPA buffer (Elpis, Daejeon, Republic of Korea) containing protease and phosphatase inhibitors (Roche, Basel, Switzerland) and incubated on ice for 30 min. The lysates were centrifuged at 20,000 $\times g$ for 20 min at 4 °C. The cell lysates were separated on SDS-PAGE gels and then transferred to cellulose membranes. The membranes were blocked in 5% (w/v) non-fat Difco™ skim milk solution in 1 \times PBS containing Tween-20 (PBST) for 1 h. The blocked membranes were incubated overnight at 4 °C with the indicated primary antibodies Supplemental Table 2. The membranes were then washed with 1 \times PBST, incubated with the appropriate secondary anti-rabbit or anti-mouse horseradish peroxidase-conjugated antibody (Thermo Scientific, Rockford, IL, USA) for 1 h, and visualized using the Chemi-Doc system (Bio-Rad) with an enhanced chemiluminescence detection reagent (Thermo Scientific).

2.8. Chromatin immunoprecipitation assay

Cells (5×10^6) were seeded in 10-mm dishes and treated with TA, with or without OPA, at the indicated concentrations for 18 h to reach approximately 70% confluence ($\sim 2 \times 10^8$ cells). A chromatin immunoprecipitation (ChIP) assay was carried out by following a previously described method [22]. Briefly, cells were initially treated with PBS containing 1% formaldehyde for 10 min, washed twice with cold PBS, and then incubated with 100 mM Tris (pH 9.4) and 10 mM DTT at 30 °C for 15 min. The cells were then rinsed twice in PBS and resuspended in 600 μ L of SolA [10 mM HEPES (pH 7.9), 0.5% NP-40, 1.5 mM MgCl₂, 10 mM KCl, and 0.5 mM DTT] by pipetting. After a short spin, the pellets were resuspended in SolB [20 mM HEPES (pH 7.9), 25% glycerol, 0.5% NP-40, 0.42 M NaCl, 1.5 mM MgCl₂ and 0.2 mM EDTA] containing protease inhibitors, followed by vigorous pipetting to extract nuclear proteins. After centrifugation at 13,000 rpm for 30 min, the nuclear pellets were resuspended in

immunoprecipitation buffer [1% Triton X-100, 2 mM EDTA, 20 mM Tris-HCl (pH 8.0), 150 mM NaCl and protease inhibitors], and chromatin was broken by micrococcal nuclease digestion using a Pierce Agarose ChIP Kit (Thermo Fisher Scientific) into fragments of 0.5–1.0 kb average length. The ChIP assays were then performed using the indicated antibodies essentially as described (Supplemental Table 1) but without SDS in all buffers. The primers used for ChIP assays are listed in Supplemental Table 2. All reactions were normalized relative to input activities and are presented as the mean \pm SD of three independent experiments.

2.9. Cell and liver tissue fractions

Cells were seeded at a concentration of 5×10^6 in 10-mm dishes. When the cells had reached approximately 70% confluence ($\sim 2 \times 10^8$ cells), they were treated with OPA with or without TA at the indicated concentrations for 18 h. Harvested cells were lysed in lysis buffer [10 mM Tris (pH 7.4), 10 mM NaCl, 3 mM MgCl₂, 0.5% NP-40, and protease inhibitor cocktail (Roche)] at 3,000 rpm and 4 °C for 3 min and the resulting supernatant was removed. Pellets were incubated in lysis buffer again on ice for 20 min, centrifuged at 4,000 rpm for 5 min at 4 °C. The resulting supernatants were used as cytosolic fractions and the pellets were used as nuclear fractions. Extraction buffer [20 mM Tris (pH 7.9), 0.42 M KCl, 0.2 mM EDTA, 10% glycerol, 2 mM DTT, and protease inhibitor cocktail] was added and the pellets were resuspended five times using a syringe, incubated on ice for 20 min, and then centrifuged at 13,000 rpm and 4 °C for 20 min. Liver tissues obtained at the end of the animal experiments were washed with ice-cold PBS and lysed according to the manufacturer's protocol (Abcam, ab113474). Briefly, tissues were weighed and cut into small pieces. To obtain the cytosolic fractions, tissue pieces were homogenized in pre-extraction buffer containing DTT using a glass tissue homogenizer (Thomas Scientific, NJ, USA). Extraction buffer was added to the pellets, the extracts were incubated on ice for 15 min, and then further homogenized using a Teflon pestle (Thomas Scientific). The suspensions were then centrifuged for 10 min at 14,000 rpm and 4 °C and the supernatants were used as nuclear fractions. Each nuclear fraction was used for the HAT assays.

2.10. Animal experiments

Seven-week-old male C57/BL6 mice were purchased from Orient Bio (Sungnam, Gyenggi, Korea) and housed at the College of Medicine of Ulsan University. All animal experiments were performed in accordance with the National Institute of Health Guide for the Care and Use of Laboratory Animals and were approved by the Ulsan University Guide for the Animals Care and Use Committee (2016-02-194). A total of 40 male C57/BL6 mice were divided into four groups ($n = 10$ each, 2 mice/cage) and housed in a temperature- and humidity-controlled room with a 12-h light/dark cycle with free access to food and water. After a 1-week acclimation period, the mice were fed a Western diet (WD), containing 1% TA (w/w; TA1) or 3% TA (w/w; TA3) based on previous studies [23–25]. Mice fed a control diet (CD) without TA were used as controls. Both the CD (98121701) and WD (D12079B) were purchased from Research Diets, Inc. (New Brunswick, NJ, USA), then mixed with TA at appropriate concentrations, and provided ad libitum. The compositions of the experimental diets are shown in Supplemental Table 3. Body weights were measured at the beginning of the experiment and subsequently at 1-week intervals for 12 weeks. Similarly, the food consumption of each group was recorded at weekly intervals for 12 weeks. At the end of the experiment, mice were sacrificed by cervical dislocation under anesthesia (100 mg/kg ketamine + 5 mg/kg xylazine) and blood samples were collected via

abdominal heart puncture for serum isolation. After laparotomy, liver, retroperitoneal fat, and epididymal fat were weighed, and a portion of the liver from each mouse was fixed in 4% formalin solution for hematoxylin and eosin staining (H&E staining). The remaining livers were used for experiments as indicated.

2.11. Hematoxylin and eosin staining

Liver specimens were fixed in 4% buffered formalin, embedded in paraffin, and cut into 4–5 μm -thick sections, which were stained with hematoxylin and eosin (H&E). Lipid accumulation in livers was assessed by microscopic observation using an Eclipse 80i microscope (Nikon Instruments, Inc., Melville, NY, USA).

2.12. Measurement of triglycerides, total cholesterol, and LDL cholesterol

The levels of triglycerides (TGs), total cholesterol, and LDL cholesterol (LDL-C) in the serum were measured enzymatically using a commercial kit (Asan Pharm, Seoul, Korea).

2.13. Protein–ligand docking simulations for the E1A binding protein p300 (EP300)

To identify the active site in EP300, the three dimensional X ray crystallographic structure of EP300 was downloaded from the Protein Data Bank (<http://www.rcsb.org/pdb/home/home.do>) (PDB ID: 4BHW) [26]. Therefore, the reported 3D structure of EP300 was applied to docking simulation. The 4BHW structure used for docking simulation contains a catalytic core in p300, and the bromo (aa 1048–1167), RING (really interacting new gene) (aa 1168–1242), PHD (plant homeodomain) (aa 1243–1285), and HAT (aa 1285–1664) domains. The bromodomain regulates gene transcription via recruitment of different molecular partners and has attracted considerable interest as a promising new epigenetic target in diverse human diseases [27]. The RING and PDH domains negatively regulate p300 HAT activity and the removal of this inhibitory function results in increased HAT activity [28,29]. The HAT domain remodels chromatin to “heterochromatin” its superstructure and enables transcription of proximal genes [30]. These domains function collectively to manifest HAT activity [28].

Prior to docking TA to EP300, we investigated the docking site in other EP300-like proteins. The EP300-like proteins were searched for using the sequence alignment method of the HHblits program [31] and the position of the bound ligands of these similar proteins was mapped to pocket sites of the EP300 core active sites measured using the VMD [32] module (protein pocket calculation program, Pck; <http://schwarz.benjamin.free.fr/Work/Pck/home.htm>). We then selected the most conserved pocket position based on overlapped positions between mapped ligand binding residues and the EP300 pocket sites for the TA docking site (Supplemental Figure 1). The TA used as a ligand for docking was downloaded as a 2D structure from the PubChem site (CID: 16129878) (<https://pubchem.ncbi.nlm.nih.gov>) [33] and converted to a 3D structure using the MarvinSketch 15.7.20.0 program (<https://chemaxon.com/products/marvin>) (Supplemental Figure 2).

The docking simulations were run using the Autodock Vina 1.1.2 program (<http://vina.scripps.edu>) [34], which can dock flexible ligands into a target protein, while keeping the protein fixed. We docked TA around the backbone residues, and the C α coordinates in each backbone binding residue of the protein receptor were used for the center of the docking space. We used default options for docking simulations except box size (30 \AA^3). This is because TA has a large volume and thus necessitates a large binding space. The docked

ligand was selected in order of binding energy up to 20 ligands per box. Thus, in the case of EP300 with 15 binding residues, up to 20×15 docked ligands are generated. The docked ligand is clustered in cluster size 1 \AA to classify similar forms. From the docking results, the best docked model, which has the lowest docking energy, was selected to represent its most favorable binding mode. When selecting the lowest energy ligand in a cluster, free energy (lowest energy + $(-kT \ln N)$, k : Boltzman constant, T : Kelvin temperature, N : the number of structure in each cluster) was used to account for the number of ligands in the population.

2.14. Statistical analysis

Data were analyzed using one-way analysis of variance with Tukey's multiple comparison test, and values are expressed as the mean \pm SD. Statistical analyses were conducted using SPSS ver. 20 (SPSS, Inc., Chicago, IL, USA). Differences were considered statistically significant at $p < 0.05$.

3. RESULTS

3.1. TA has potential as a novel HATI

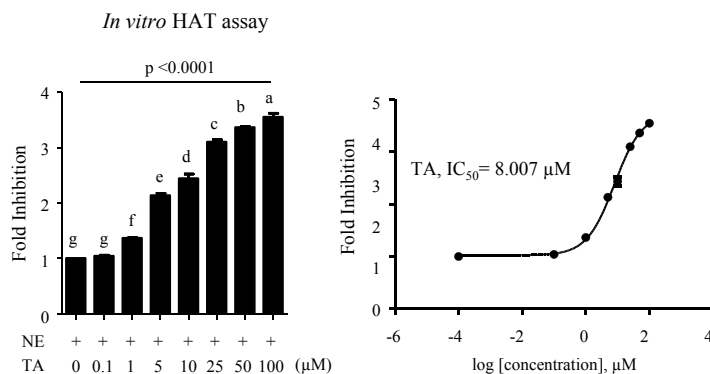
To examine whether TA modulates HAT activity, we initially measured HAT activity in a cell-free system. TA at various concentrations was incubated with a HeLa nuclear extract (NE), and epigallocatechin-3-gallate (EGCG), a well-known specific HATI [35], was used for comparison (Supplemental Information Figure 1, left panel). As shown in Figure 1A (left panel), TA significantly inhibited the HAT activity. Interestingly, the IC₅₀ values for HAT inhibition by TA (Figure 1A, right panel) and EGCG (Supplemental Figure 3, right panel) were 8.007 μM and 15.430 μM , respectively, indicating that TA might show a considerably stronger inhibitory effect than that shown by EGCG. To confirm the anti-HAT activity of TA, we examined the inhibitory effect of TA on HAT using a radiolabeled H4 tail peptide. Consistent with the results of the cell-free HAT assay, TA showed a HAT inhibitory effect in an autoradiography assay (Figure 1B). To ensure that the activity of TA was specifically directed against HATs, we initially sought to assess the effect of TA on HDAC activities. When HeLa NEs were used as a source of HDAC enzymes, deacetylase activity was not affected by the presence of TA, whereas Trichostatin A (TSA) efficiently blocked nuclear HDAC activities (Supplemental Figure 4). This result indicates that TA has no specificity for HDACs. Taken together, these data show that TA has potential as a novel HATI.

Next, we examined the enzyme specificity of TA. The HAT activities of p300, CREB-binding protein (CBP), and p300/CBP-associated factor (PCAF) HATs were measured either in the absence of TA or in the presence of increasing concentrations of TA. As shown in Figure 1C, TA was found to be a highly efficient inhibitor of p300 acetyltransferase activity, with an IC₅₀ value of 3.886 μM (Supplemental Figure 5, upper panel). Under the same conditions, TA also inhibited CBP and pCAF histone acetyltransferase activities (albeit to a lesser extent than against p300), with IC₅₀ values of 4.592 and 5.414 μM , respectively, thereby indicating that TA may be a general inhibitor of histone acetyltransferase (Supplemental Figure 5, middle and lower panels).

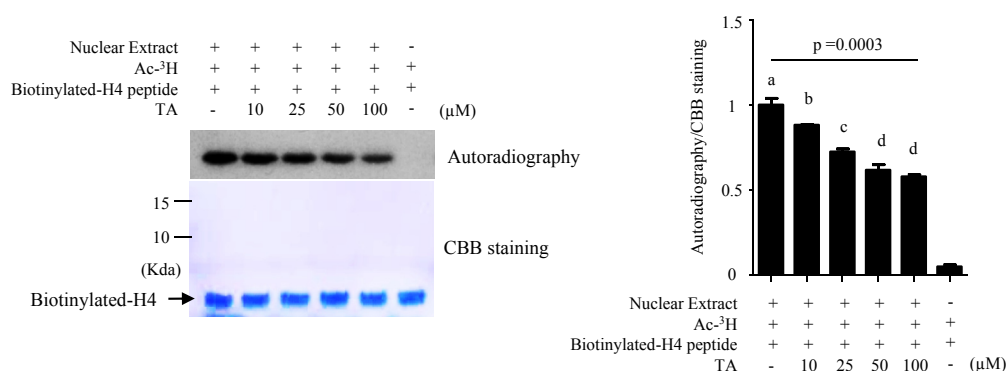
3.2. TA reduces lipid accumulation mediated by lipogenesis-related genes through inhibition of HAT activity

We next examined the anti-lipogenic effects of TA in HepG2 cells to evaluate whether TA can effectively block hepatic lipid accumulation. Oleic and palmitic acid (OPA) treatment increased the lipid

A



B



C

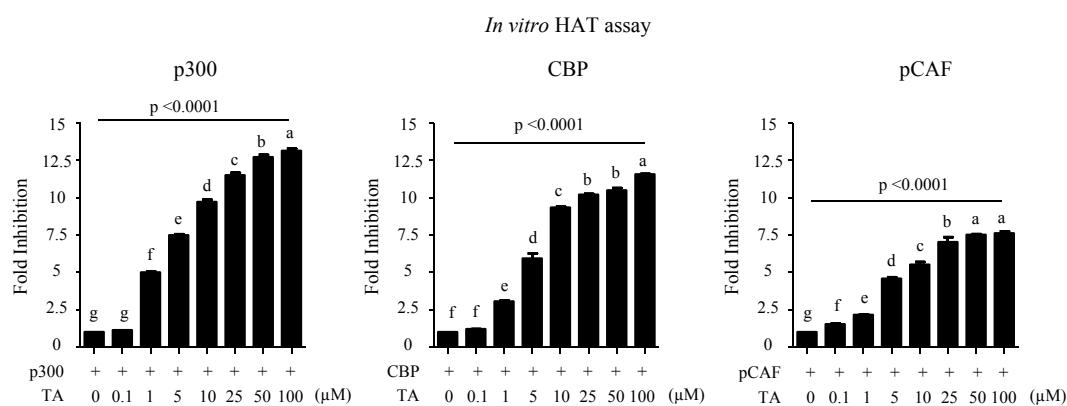


Figure 1: Inhibitory effects of TA on HAT activity. (A) A colorimetric assay was performed to measure HAT activity in the presence of TA at the indicated concentrations. The results are presented as percentages relative to the control sample, which was incubated without TA (left panel). The IC_{50} value of TA inhibition of HAT activity was calculated using Prism software (right panel). (B) An *in vitro* HAT assay using autoradiography was performed to evaluate the effect of the anti-HAT activity of TA on the acetylation of a synthetic H4 peptide by a HeLa NE. The arrow indicates histone H4 (left panel). The autoradiography was quantified using Image J software (right panel). The values presented are the means \pm SD of two independent experiments. Means with different superscript letters are significantly different, $p < 0.05$. (C) Inhibitory effect of TA on global HAT. Enzyme-specific anti-HAT activities of TA against p300, CBP, and PCAF were measured using purified enzymes. A colorimetric assay was performed to measure enzyme activities in the presence of TA at the indicated concentrations. The results are presented as percentages relative to the control sample. The values presented are the means \pm SD of three independent experiments. Means with different superscript letters are significantly different, $p < 0.05$.

accumulation in HepG2 cells by approximately 160% and, importantly, TA attenuated the OPA-induced lipid accumulation (Figure 2A). To exclude the possibility that the effect was due to TA cytotoxicity, we performed a cell viability assay (Supplemental Figure 6). TA did not cause obvious cytotoxicity even at the maximum concentration used. Next, qRT-PCR was performed to determine whether TA is involved in regulation of the lipogenesis-related genes sterol regulatory element-binding protein 1c (*SREBP-1c*), ATP-citrate lyase (*ACLY*), fatty acid synthase (*FASN*), and peroxisome proliferator-activated receptor gamma (*PPAR γ*). As expected, OPA significantly increased the mRNA expression of these genes, whereas TA prevented the increase and also abrogated their protein expression (Figure 2B,C). To elucidate the relationship between mRNA expression of the lipogenic genes and HAT

activity, we incubated HepG2 cells, in the presence or absence of OPA, with C-646, a specific p300/CBP inhibitor, at the indicated concentrations (Figure 2D). mRNA expression of the lipogenic genes was abrogated by blocking the p300/CBP activity using C-646. Collectively, our data indicate that TA ameliorates lipid accumulation through inhibition of lipogenic genes, via its anti-HAT activity.

3.3. TA attenuates OPA-induced hyperacetylation of both histones and total proteins through its anti-HAT activity

To evaluate whether the anti-lipogenic properties of TA are correlated with its anti-HAT activity, we initially examined HAT activity in HepG2 cells. Cells were cultured with OPA in the presence or absence of TA at the indicated concentrations, and total HAT activity was measured in

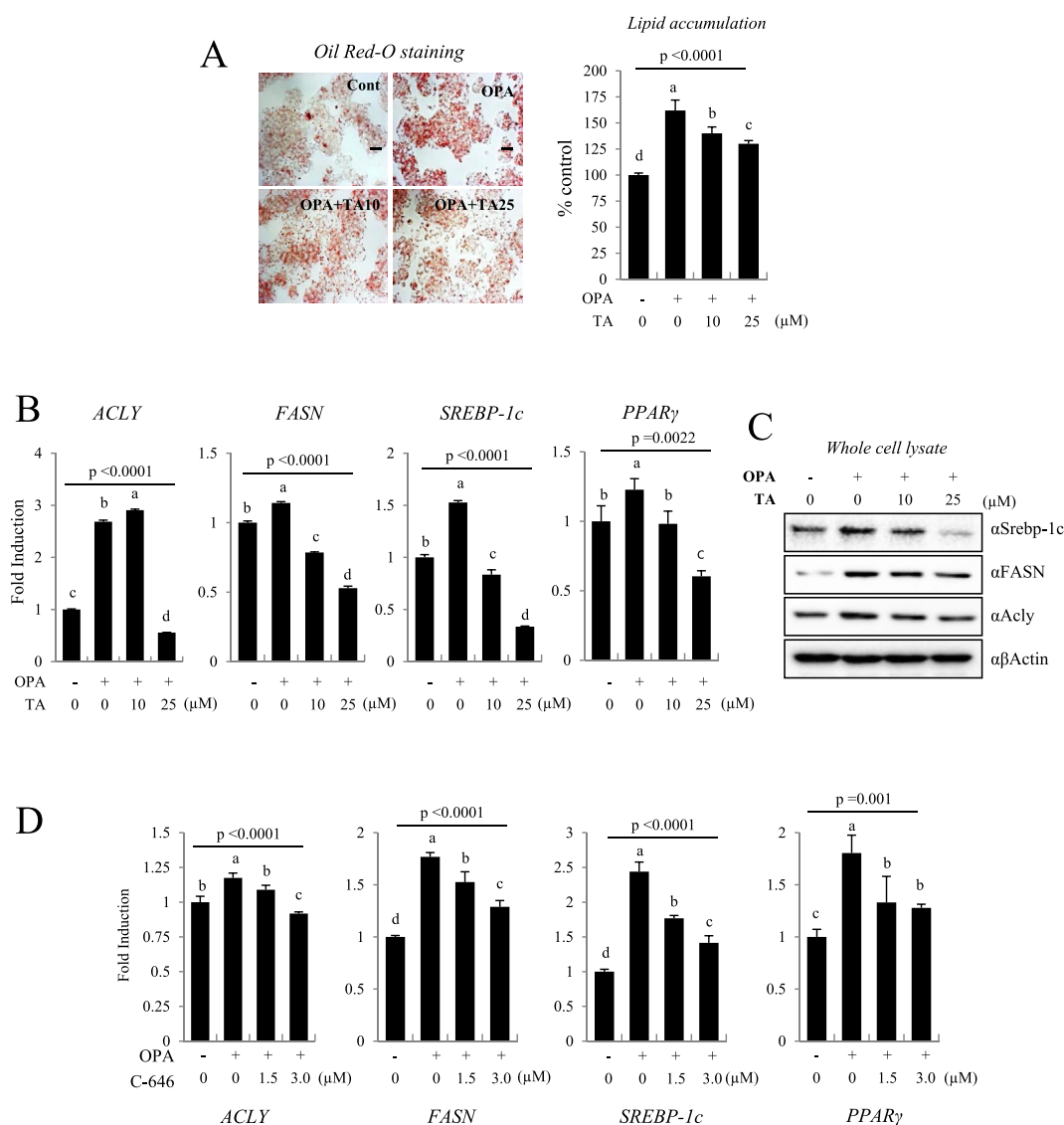


Figure 2: TA attenuated lipid accumulation in HepG2 cells. (A) OPA-induced lipid accumulation was significantly inhibited by TA. HepG2 cells treated with TA, in the presence or absence of OPA, were stained with an Oil Red O solution (left panel). Representative photographs were captured, and staining was quantified (right panel). (B) TA inhibited the mRNA expression of lipogenic genes. The mRNA expression of *ACLY*, *FASN*, *SREBP-1c*, and *PPAR γ* was measured by qRT-PCR. (C) TA prevented the OPA-induced protein expression of *SREBP-1c*, *FASN*, and *ACLY*. Western blot analysis was performed using the indicated antibodies. (D) C-646, a specific inhibitor of p300/CBP, blocked the OPA-induced mRNA expression of lipogenic genes. HepG2 cells were treated with C-646 at the indicated concentrations in the presence or absence of OPA for 18 h. mRNA expression of *ACLY*, *FASN*, *SREBP-1c*, and *PPAR γ* was measured by qRT-PCR. The values presented are the means \pm SD of three independent experiments. Means with different superscript letters are significantly different, $p < 0.05$.

isolated nuclear fractions. HAT activity in the OPA-treated cells was significantly higher than that in the control group, and was inhibited by TA (Figure 3A). To examine whether the TA-mediated reduction in HAT activity affected protein lysine acetylation, we evaluated acetylation at Lys residues in a whole-cell lysate and a histone extract from HepG2 cells. Acetylation at Lys residues in total proteins was increased by OPA, whereas TA effectively attenuated this (Figure 3B). Moreover, compared with that in the control, TA inhibited the acetylation of histones H3K9 and H3K36 (Figure 3C), indicating that the anti-HAT activity of TA effectively blocks the acetylation of both total proteins and histone H3 tails, which are involved in NAFLD [36,37].

3.4. TA blocks hyperacetylation of H3K9 and H3K36 in the promoters of both *FASN* and *ACLY*

Lysine acetylation of histones in promoter regions neutralizes their positive charge and induces conformational changes in DNA, thereby increasing the transcriptional activation of genes [38]. Hyperacetylation of histones in the promoter regions of the *FASN* and *ACLY* genes is responsible for upregulation of the transcriptional activity of these genes, resulting in lipid accumulation. To elucidate whether TA modulates the acetylation of histones in the promoters of the *FASN* and *ACLY* genes, we performed chromatin immunoprecipitation (ChIP) assays and also examined the occupancy of p300, a transcriptional

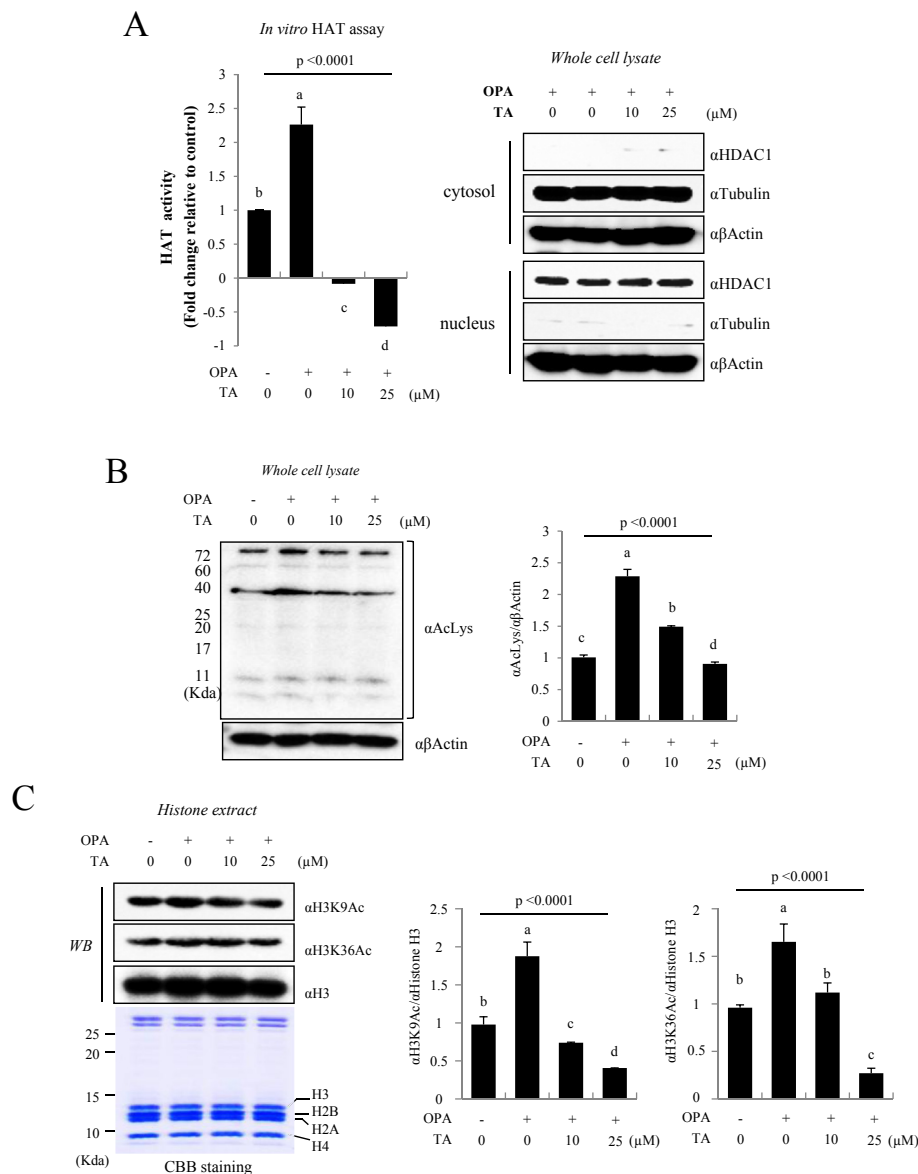


Figure 3: TA prevented the OPA-induced hyperacetylation in HepG2 cells. (A) The HAT activity was measured in an NE from HepG2 cells. Activity in each group is presented as a percentage relative to that in the control group, which was incubated without OPA and TA. The values presented are the means \pm SD of three independent experiments. Means with different superscript letters are significantly different, $p < 0.05$ (left panel). To confirm nuclear fraction, western blotting was carried out. HDAC1 and tubulin were used as nuclear and cytosolic markers, respectively (right panel). (B, C) TA blocked the hyperacetylation of total proteins and histone proteins. HepG2 cells were treated with TA, in the presence or absence of OPA. Total proteins and core histones were extracted from the cells, and the acetylation status was determined. To confirm the histone extraction, CBB staining was carried out. The expressions of proteins were quantified using Image J software. The quantified values presented are the means \pm SD of three independent experiments. Means with different superscript letters are significantly different, $p < 0.05$.

coactivator. As shown in Figure 4, OPA effectively induced acetylation of the histones H3K9 and H3K36 near the sterol regulatory element (SRE) regions of *FASN* and *ACLY*. The increased acetylation status of the SRE of *FASN* was significantly diminished by 10 μ M and 25 μ M TA (Figure 4, upper panel), whereas increased histone H3K9 and H3K36 acetylation in the SRE of the *ACLY* promoter was significantly decreased only by 25 μ M TA (Figure 4, lower panel). It was also observed that the occupancy of p300, which is responsible for histone acetylation, differed between the two genes. p300 was bound to the *FASN* promoter with a pattern similar to the H3K9 and H3K36 acetylation status of the *FASN* promoter region, whereas binding of p300 to the *ACLY* promoter was also diminished by 25 μ M TA (Figure 4, upper and lower panels, respectively). Collectively, our results indicate that TA abrogates occupancy of p300 in the SRE of both *FASN* and *ACLY* genes, subsequent to inhibition of the OPA-induced hyperacetylations on histone H3K9 and H3K36 in this region.

3.5. TA ameliorates the pathogenic features of NAFLD in vivo

To confirm that TA attenuates lipid accumulation and ameliorates the various pathogenic features of NAFLD, we fed mice either a CD

or WD with or without 1% or 3% TA supplementation (Supplemental Table 3). Mice in the WD group showed a higher average body weight compared with those in the CD group, whereas the mice group fed the WD containing 3% TA had a low average body weight that was comparable to that of mice in the CD group (Figure 5A). Although food intake was increased in the WD groups in the presence of TA (Figure 5E), the average body weight gain in the 3% TA group was lower than that in the WD-fed group (Figure 5B). To determine whether this observed weight gain was associated with an increase in the size and weight of the liver, epididymal fat, and retroperitoneal fat, we compared these measurements among the groups. As shown in Figure 5C, not only was the size of these tissues enlarged but also their weights were significantly increased in the WD group at 12 weeks ($p < 0.01$). Furthermore, in H&E-stained liver tissue, lipid accumulation was observed to be higher in the WD-fed mice than in the CD group, and the liver tissues in mice fed the 3% TA-supplemented diet exhibited reduced lipid droplet accumulation compared with that in the WD-fed mice. Lipid accumulation in the 3% TA-supplemented mice was also comparable to that in the CD-fed mice (Figure 5D). The triglyceride (TG), total

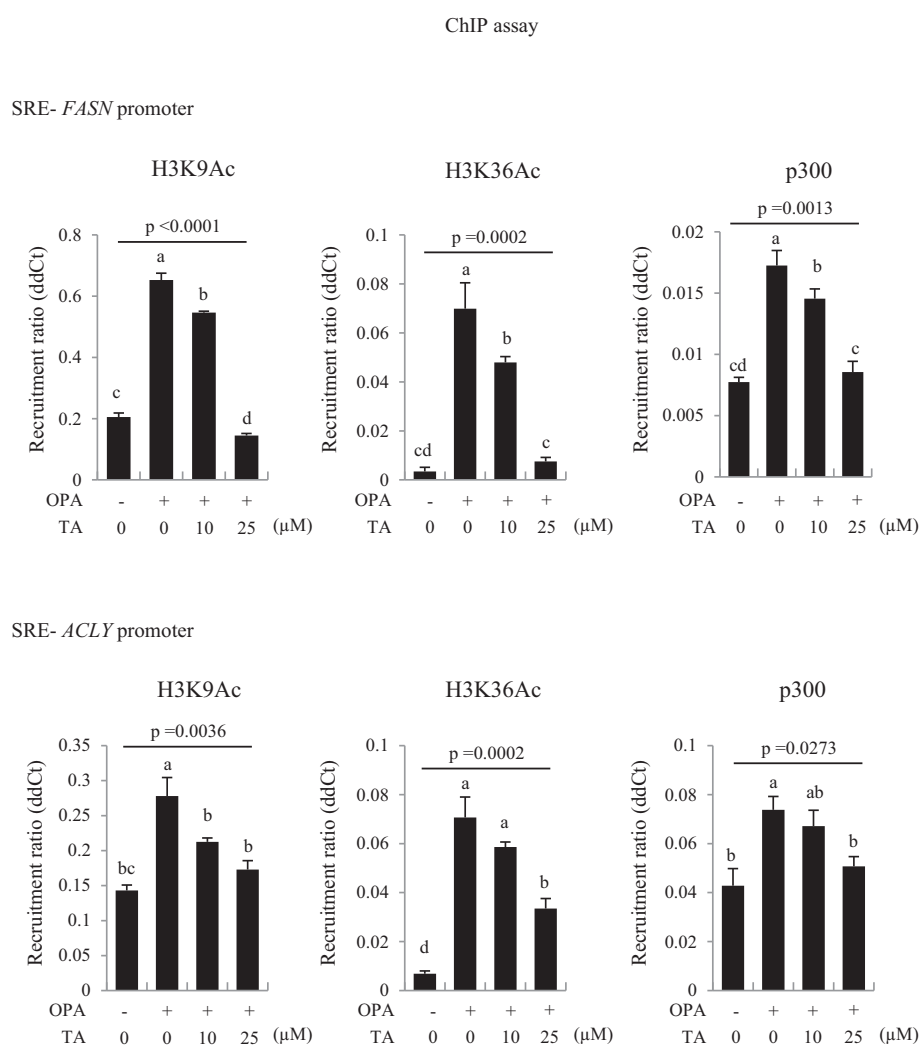


Figure 4: TA inhibited the acetylation of histones H3K9 and H3K36 in the promoter regions of *FASN* and *ACLY*. HepG2 cells were treated with TA, in the presence or absence of OPA for 18 h, and a ChIP assay was performed using the indicated antibodies. The precipitated samples were analyzed by qRT-PCR. The values presented are the means \pm SD of three independent experiments. Means with different superscript letters are significantly different, $p < 0.05$.

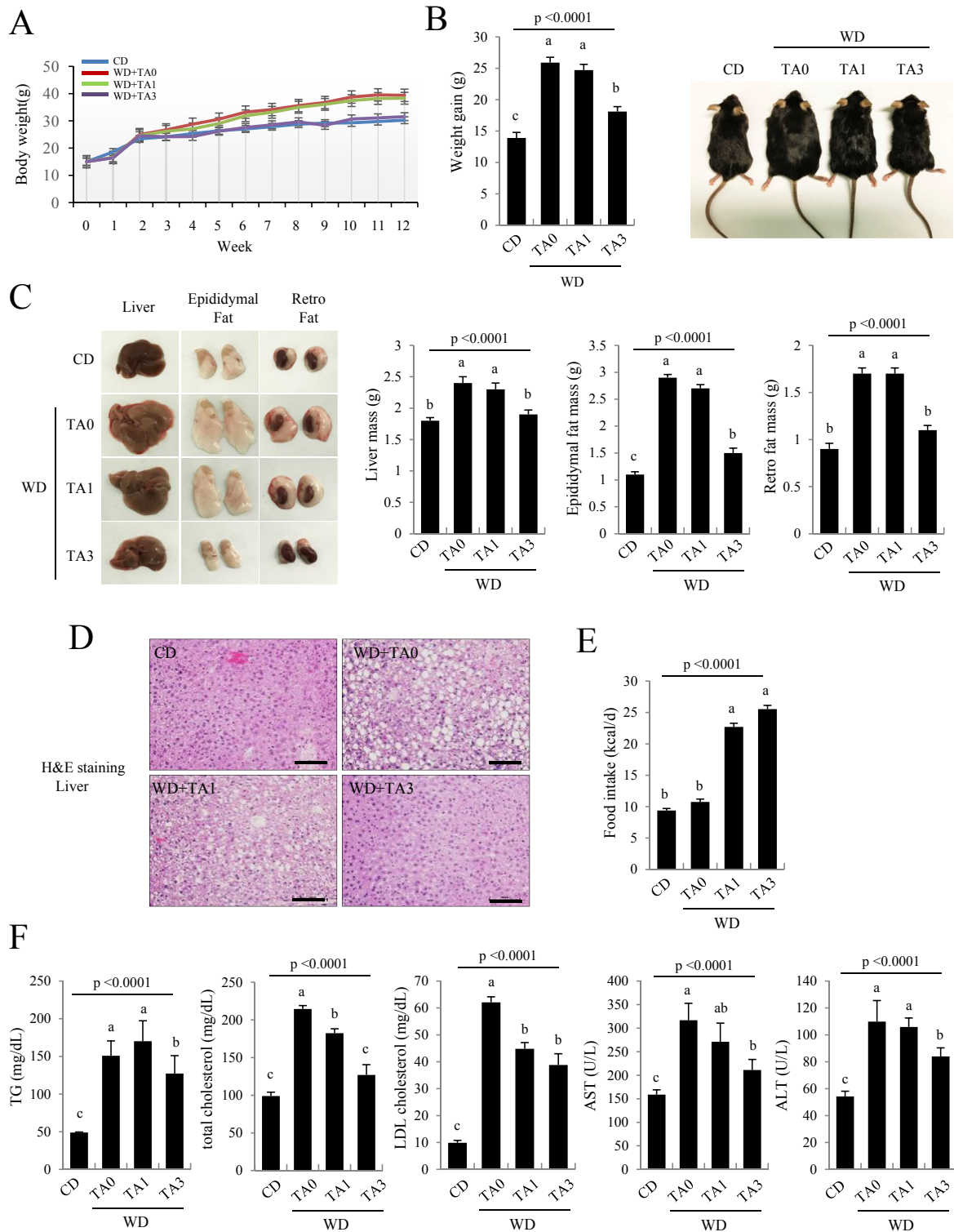


Figure 5: TA attenuated WD-induced NAFLD features in mice. (A) Body weight changes in the mice fed WD with or without TA for 12 weeks ($n = 10$ /each group). (B) Body weight gain (left panel) and representative images of the mice fed WD, with or without TA, for 12 weeks ($n = 10$ /each group, right panel). (C) Representative images of the liver, epididymal fat, and retroperitoneal fat in the mice fed WD, with or without TA, for 12 weeks (left panel). The average values for the liver, epididymal, and retroperitoneal fat mass after 12-week TA supplementation are presented as the means \pm SD ($n = 10$ /each group, right panel). (D) After a 12-week TA supplementation, H&E staining of mouse liver specimens was performed. Representative images are shown (scale bar = 100 μ m). (E) Daily food intake for a 12-week TA supplementation ($n = 8$ /each group). The values presented are the mean \pm SE. Means with different superscript letters are significantly different, $p < 0.05$. (F) Serum levels of TGs, total cholesterol, LDL-C, AST, and ALT were measured after a 12-week TA supplementation ($n = 8$ /each group). TA0, mice fed WD only; TA1, mice fed WD supplemented with 1% TA; TA3, mice fed WD supplemented with 3% TA. The values presented are the mean \pm SE. Means with different superscript letters are significantly different, $p < 0.05$.

cholesterol, and LDL cholesterol (LDL-C) levels were significantly lower in both 1% and 3% TA-supplemented groups than in the WD control group (Figure 5F). The increased levels of aspartate transaminase (AST) and alanine transaminase (ALT) in the WD-fed mice group were also improved by supplementation with 3% TA (Figure 5F). These results establish that dietary supplementation with TA ameliorates NAFLD pathogenic features in vivo.

3.6. TA decreased the mRNA expression of lipogenesis-related genes by hypoacetylation of H3K9 and H3K36 via its anti-HAT activity in vivo

Finally, to confirm that the TA-mediated improvement of NAFLD in vivo was due to its anti-HAT activity, we examined the anti-HAT activity of TA in vivo. Initially, the HAT activity was measured in NEs prepared from mouse livers after dietary supplementation of the CD or WD with or without TA for 12 weeks. Consistent with the previous in vitro results (Figure 3A), HAT activity was increased in the WD-fed mice, and TA attenuated this increase (Figure 6A). In addition, the Lys acetylation levels in the whole-cell extracts from mouse livers were significantly higher in the WD-fed mice than in the CD group mice and were attenuated by TA supplementation (Figure 6B). The acetylation of histones H3K9 and H3K36 was also significantly lower in the 3% TA-supplemented group than in the WD-fed mice (Figure 6C). Moreover, mRNA expression of mouse lipogenic genes such as *DGAT2*, *FASN*, *SREBP-1c*, and *PPAR γ* was also decreased in the TA-supplemented mice (Figure 6D). Taken together, our findings indicate that dietary supplementation with TA induces hypoacetylation of histone and non-histone proteins through its anti-HAT activity, resulting in the mRNA expression of lipogenesis-related genes in vivo.

3.7. Docking simulation between EP300 and TA

Finally, we searched the possible ligand binding site of EP300-like proteins to determine the TA docking position of EP300 because protein structures with similar sequences are often consistent in function and shape. As a result of the sequence alignment, we found a total of 1,189 template structures (EP300-like proteins) and examined the binding sites of 483 ligands in the template structures (Supplemental Figure 6). The most probable binding site from the EP300-like protein was located in a pocket for the bromo domain, and the most conserved ligand binding positions from EP300-like protein is the pocket number 66 (Supplemental Figure 6, orange color of right panel), and the pocket residues are PRO1074, PHE1075, GLN1077, VAL1079, LEU1084, ILE1086, TYR1089, MET1097, ASP1098, MET1124, ASN1127, ALA1128, TYR1131, ASN1132, and VAL1138, and then we docked the TA to these residues (see the methods and materials for detail information).

We identified that the top five docked ligands bound to around the bromo domain of EP300 in buried form (Figure 7A), which have the free energy values between -8.78 kcal/mol and -9.17 kcal/mol (Supplemental Figure 7). Particularly, the most possible binding residues of EP300 for TA are containing ASN1126, TRP1129, LEU1130, TYR1139, LYS1140, SER1143, LYS1144, SER1146, GLU1147, GLU1150, LYS1167, GLU1169, PHE1170, SER1171, ARG1187, ASP1188, LYS1235, ASP1237, LEU1239 and PRO1453 (Figure 7 B), forming 13 hydrogen bonds with the EP300 protein to form a stable structure (Figure 7C and Supplemental Figure 8). Altogether, TA binds to a pocket between bromo and RING domain of p300, possibly reducing its HAT activity through inducing conformational change of p300.

4. DISCUSSION

Epigenetic dysregulation is known to initiate the development of various human diseases and to contribute to their progression. Although epigenetic modulation including HDACi and DNA methyltransferase inhibition has been extensively studied, and several are currently being assessed in clinical trials [39], there is little information available on HAT inhibitors. HAT is a plausible target for preventive or therapeutic agents [40,41], and there are now several known HATi derived from natural products [42–44] that have favorable safety profiles [45]. EGCG, the major polyphenol found in green tea, has potent anti-HAT activity, with global specificity for the majority of HAT enzymes [35]. In addition, previous studies have shown that garcinol inhibits p300 and PCAF in vitro and in vivo, whereas anacardic acid inhibits TIP60 as well as p300 and PCAF, and curcumin inhibits p300 and PCAF, suggesting that dietary compounds are potent epigenetic regulators, particularly via HAT inhibition [42]. However, to our knowledge, epigenetic regulation by TA has not previously been investigated, and thus the present study is the first to indicate that TA is a potent and specific HATi.

Initially, we demonstrated the anti-HAT activity of TA. TA showed global specificity for the majority of HAT enzymes examined, but not other epigenetic enzymes, i.e., HDACs, illustrating that TA is a specific HATi. A previous acetylation study identified an astonishing 978 acetylated proteins in human liver tissue [46], indicating that protein acetylation is involved in a broad range of cellular activities in the liver. To date, substantial evidence has indicated the involvement of HAT activity in NAFLD [13,47]. Using qRT-PCR analysis, we observed that C-646 treatment leads to a decrease in the mRNA expression of lipogenic genes related to NAFLD, supporting the notion that p300-induced HAT activity causes NAFLD. Although TA has been shown to have an inhibitory effect on lipid accumulation in the liver [48,49], there has been no evidence that TA suppresses the HAT-mediated acetylation of histone and non-histone proteins and the subsequent expressions of lipogenesis-related genes. In the present study, in vitro and in vivo HAT assays clearly showed the TA inhibits HAT-induced histone acetylation. The acetylation of histone H3K9 is well known as an epigenetic marker for NAFLD [47,50], and, as previously remarked, acetylation of proteins is associated with dynamic cellular activities in the liver [46]. In addition, we showed that TA attenuated the lipid accumulation-induced increase in acetylation levels of total proteins and histones H3K9 and H3K36 in vitro and in vivo. Thus, our study provides firm evidence to support the notion that TA suppresses HAT-mediated acetylation of both histone and non-histone proteins.

The hyperacetylation of histone proteins by HATs is known to be associated with gene activation [51]. In particular, p300, which is a transcription factor having HAT activity, links activators to the transcription machinery at promoters [52]. The p300/CBP complex dynamically regulates hundreds of different transcription factors, including *SREBP-1c* and *PPAR γ* [53,54]. Glucose-induced p300/CBP activation contributes to the development of NAFLD through enhanced activation of lipogenic genes [55]. Indeed, numerous studies have shown the relationship between lipogenic gene expression and NAFLD, as well as the preventive effects of natural compounds [56,57]. Our data indicated that the mRNA expression of lipogenic genes was increased during lipid accumulation in vitro and in vivo. In addition, consistent with some previous studies [48,58,59], we observed that TA downregulated the mRNA expression of lipogenic genes. Importantly, in contrast to previous studies, we provide direct evidence to explain the observed responses based on an epigenetic mechanism. A recent

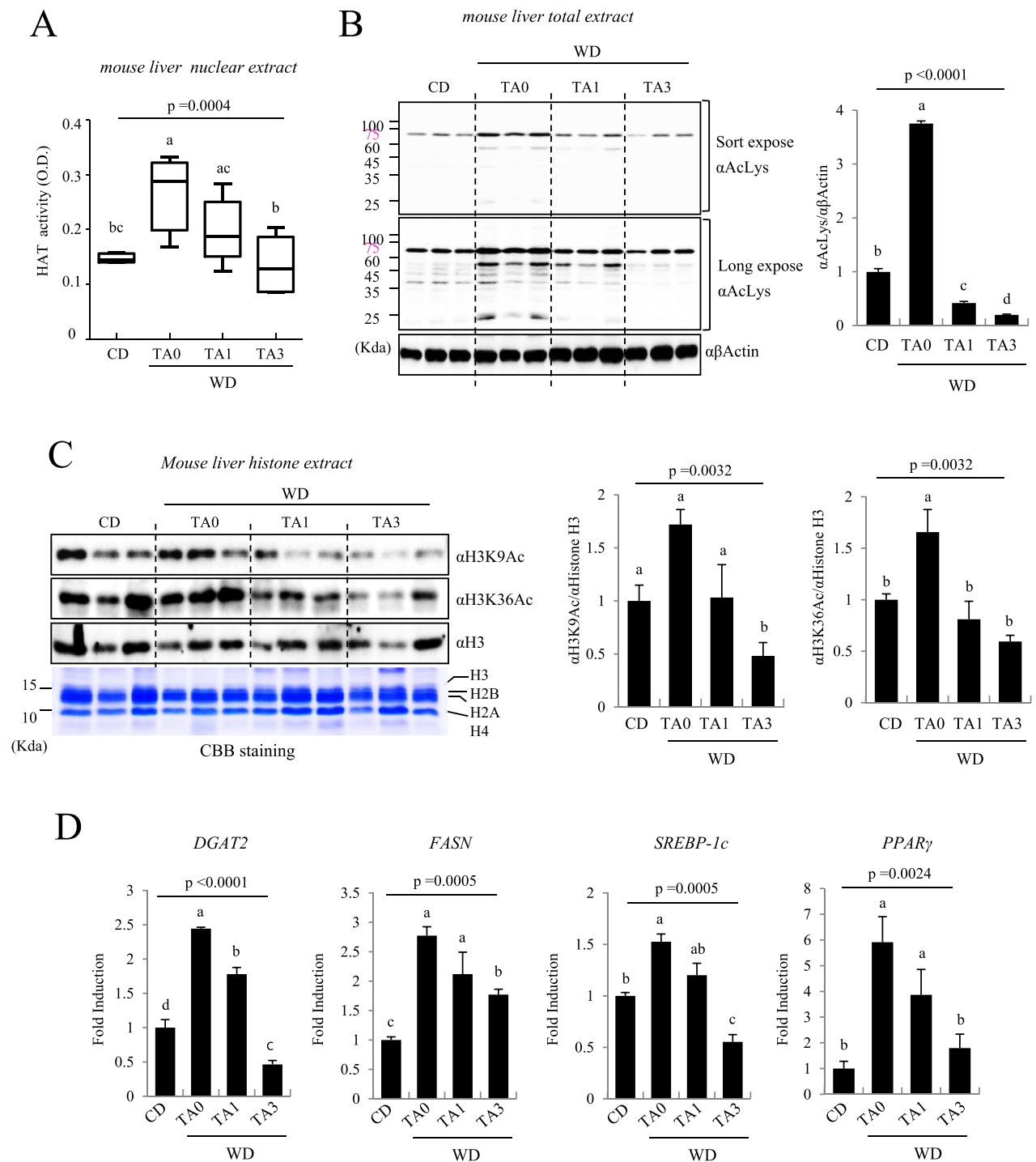


Figure 6: TA prevented WD-induced hyperacetylation and mRNA expression of lipogenic genes in mice. (A) TA suppressed the WD-induced HAT activity, measured in NEs derived from mouse livers after a 12-week TA supplementation ($n = 10$ /each group). The average OD values presented are the means \pm SD. Means with different superscript letters are significantly different, $p < 0.05$. (B) TA decreased the WD-induced acetylation of hepatic proteins in mouse livers. After a 12-week TA supplementation, the total acetylation status was determined in whole-cell lysates of the mouse livers (left panel). The expressions of acetyl-Lys were quantified by normalizing intensity values to that of the internal control $\alpha\beta$ -actin ($n = 3$ /each group, right panel). The values presented are the means \pm SE. Means with different superscript letters are significantly different, $p < 0.05$. (C) TA blocked the WD-induced histone acetylation. After a 12-week TA supplementation, core histones were extracted from mouse livers, and the acetylation status at specific Lys sites on histone H3 tails was determined using the indicated antibodies. The acetylation of histones H3K9 and H3K36 was quantified by normalizing intensity values to the expression density of total histone H3 ($n = 3$ /each group, right panel). The values presented are the means \pm SE. Means with different superscript letters are significantly different, $p < 0.05$. (D) TA inhibited the mRNA expression of lipogenic genes in mouse livers. After a 12-week TA supplementation, the mRNA expression of *Dgat2*, *Fasn*, *Srebp-1c*, and *Ppar γ* was measured by qRT-PCR. The values presented are the means \pm SD. Means with different superscript letters are significantly different, $p < 0.05$.

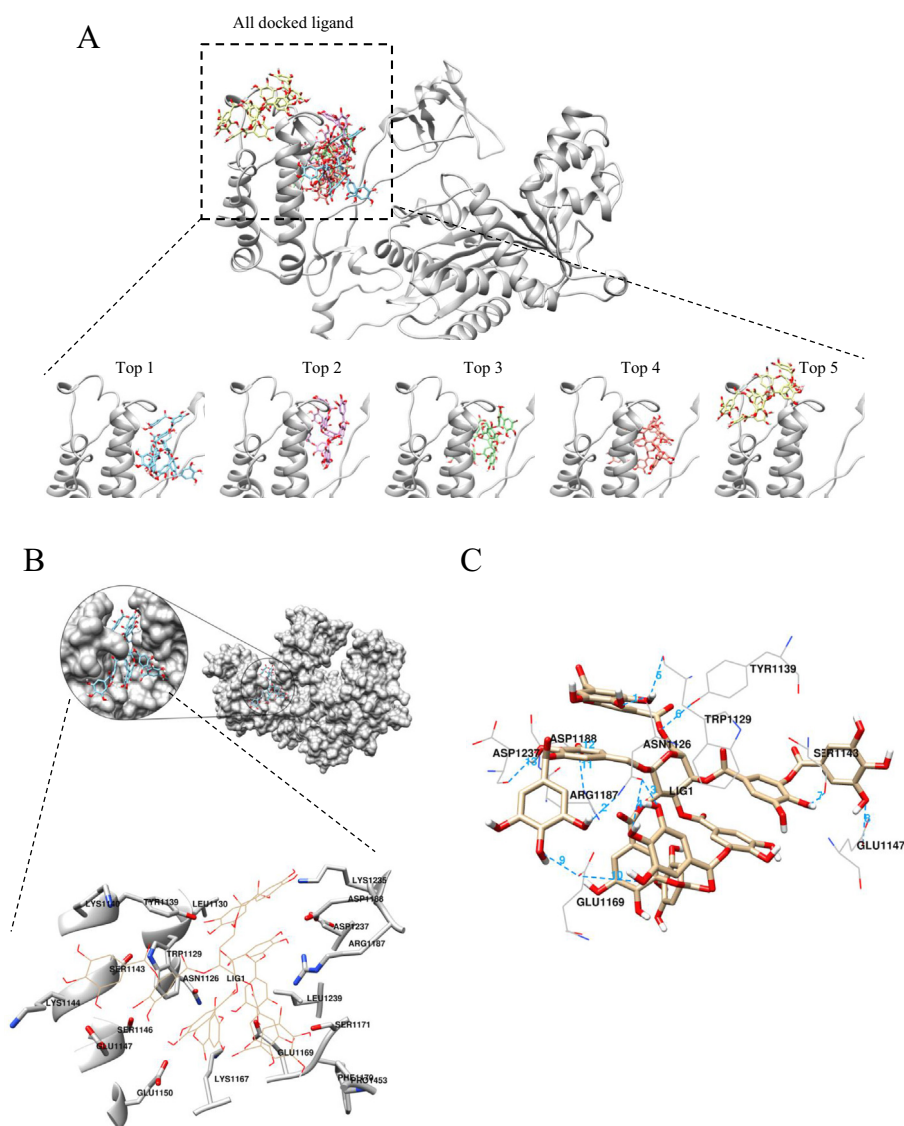


Figure 7: Interacting site and hydrogen bond of the top docking result. (A) Top five docking results of TA to EP300. Gray ribbon, p300; TA structure is presented as a cylinder mode. (B) The top ligand is located between the bromo and RING domains of EP300. The target protein is represented by gray surface area and the ligand is represented by sticks. (B) The most possible interacting site. When selecting the lowest energy ligand in the cluster, free energy (lowest energy + $(-kT \ln N)$, k : Boltzman constant, T : Kelvin temperature, N : the number of structures in each cluster) was used to account for the number of ligands in the population. (C) Hydrogen bonds of the top docking result. The ligand is marked with sticks and the residues of the protein are indicated with a gray wire frame. Hydrogen bonds, of which there are 13, are shown as blue dotted lines. To identify the active site in p300, the three dimensional X ray crystallographic structure of p300 was downloaded from the Protein Data Bank (<http://www.rcsb.org/pdb/home/home.do>) (PDB ID: 4BHW). The 3D structure of TA (PubChem CID: 16129878), the ligand to be used for docking, was generated using Marvin sketch (<https://chemaxon.com/products/marvin>). The docking simulation was run using Autodock Vina 1.1.2 (<http://vina.scripps.edu>). All structures were drawn using Chimera software.

study showed that the HAT enzyme p300, bound to the *FASN* promoter, increases histone acetylation in this region, and eventually increases mRNA expression of the *FASN* gene [60]. Consistent with these observations, our data also showed that histone acetylation was increased in the *FASN* promoter during lipogenesis and, using ChIP assays, we further demonstrated that TA modulated this process. These findings provide important evidence in support of our hypothesis. Unexpectedly, however, not only was the recruitment of p300 to the SRE region of the *ACLY* promoter not inhibited but also acetylation of H3K9 and H3K36 was not significantly abrogated by treatment with 10 μ M of TA, suggesting that the *ACLY* gene is less vulnerable to epigenetic regulation by TA. Another plausible explanation is that increased *ACLY* expression promotes histone acetylation by generating

acetyl-CoA [61], which plays an essential role in determining the overall status of histone acetylation in mammalian cells [46,62]. Finally, we adopted a WD-induced NAFLD model to confirm whether TA-induced inhibition of HAT activity prevents development of the pathogenic features of NAFLD. Two previous studies have reported that histone acetylation is influenced by a WD [63,64], suggesting the possibility of preventing WD-induced diseases through the regulation of HAT activity. As previously mentioned, our results showed that dietary TA supplementation not only ameliorated WD-induced hyperacetylation of histone and non-histone proteins in the liver tissues but also attenuated NAFLD-induced phenotypes and clinicopathological characters, even though food intake was increased in the TA-fed mice, thereby supporting our hypothesis that WD-induced disease could be regulated by the control of

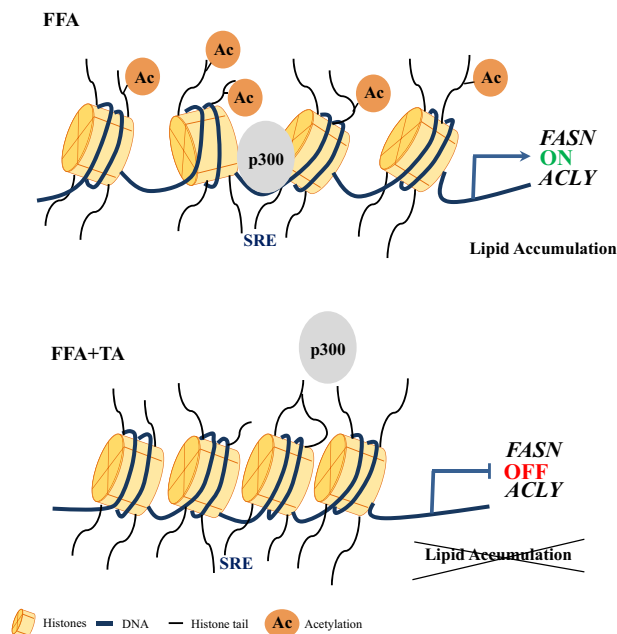


Figure 8: Schematic representation of the potential mechanism of action of TA against NAFLD. TA abrogates excess lipid accumulation in hepatic cells owing to its HATI activity. As a potent and novel HATI, TA can potentially prevent NAFLD development via inhibition of HAT activity. TA abrogates the binding of p300, as a representative HAT, to the SRE region of the *FASN* and *ACLY* promoter, and consequently prevents hyperacetylation around this region. Finally, TA-mediated hypoacetylation of histones blocks the mRNA expression of *FASN*- and *ACLY*-related genes and impedes lipid accumulation in hepatic cells. Thus, TA represents a promising candidate dietary compound for the prevention of NAFLD.

HAT activity. Animals fed high-TA-containing diets have a higher total feed intake than those fed a low-TA-containing diet, and the groups on high-TA diets showed a significant decrease in weight gain [65,66]. In this regard, a study on the biochemical mechanism underlying the activity of TA demonstrated that the major effect of TA was not related to the inhibition of food consumption. Instead, it has been demonstrated that the effects of TA are mediated via the efficiency with which digested and absorbed nutrients are converted into new body substances [67], indicating that this phenomenon could be due to a direct inhibitory effect on a key metabolic pathway or indirect effect related to the diversion of metabolism by TA. On the basis of the findings of these previous studies and our present data, it can be postulated that the preventive effects of TA on the development of NAFLD in vivo are related to TA-induced epigenetic regulation of lipid metabolic pathways. We have also demonstrated a feasible mechanism by which the relative occupancy of p300 in the promoter regions of SREBP1c-regulated genes determines overall *FASN*- or *ACLY*-mediated mRNA expression, indicating that TA, as a novel HATI, has the important effect of regulating lipid metabolism. By extension, to explain the mode of action of TA as a HATI, we predicted a possible p300-TA docking model (Figure 7, and Supplemental Figures 3–6). The results showed that TA interacts with a catalytic pocket, bromodomain, and RING domain in p300, and regulates gene transcription by binding directly to histone H3 and negatively regulates itself via an autoinhibitory function [28], indicating that TA may interrupt the function of p300 by inducing a conformational change. Taken together, the results of this study suggest the potential application of a new class of TA nutraceuticals having HATI activity.

In summary, we have provided evidence that TA, a novel HATI, inhibits the acetylation of histone and non-histone proteins and activation of

the mRNA expression of lipogenesis-related genes both in vitro and in vivo (Figure 8), indicating that inhibition of HAT activity by TA is necessary for the prevention of NAFLD. Nevertheless, despite our growing awareness of the value of TA as a phytochemical, issues regarding its practical application remain to be addressed. In this regard, the present study can be considered to have certain limitations. First, notably, we have not provided an explanation for the nuclear-specific effects of TA. TA rarely penetrates the plasma membranes of intact cells, but here we should emphasize that TA enters previously injured cells only through the damaged portions of the cell membrane [68]. Accordingly, to explain the nuclear-specific effects of TA, it would be possible to envisage a scenario whereby TA penetrates membranes damaged by WD-induced excessive oxidative stress [69,70] and thereafter forms a complex with p300 in cytoplasm, and this complex is subsequently translocated to the nucleus. In this regard, a recent study has shown the translocation of p300 from the cytoplasm to nucleus via activation of the RhoA-Akt axis pathway, which is closely associated with lipid metabolism [71]. Second, although cytotoxicity was not observed at the concentrations used in our in vivo and in vitro studies, it is conceivable that the concentrations of TA used in the present study lack physiological relevance. Lastly, we did not elucidate the causes that induce discordance between food intake and weight gain in the mice fed TA-containing diet, although the possibility was addressed based on the previous reports showing the same result with our study. However, it is important to determine the energy where is being absorbed and expended metabolically. Given the importance of the aforementioned limitations of this study, further relevant in-depth studies should be conducted.

AUTHOR CONTRIBUTIONS

H.-K.C. conceived and designed the experiments; M.-Y.C., J.-T.H., J.-H.S., S.-H.L. and E.-J.S. performed the experiments; H.-K.C., J.-H.P., and J.-T.H. analyzed the data; J.H.L. carried out the TA-EP300 docking simulation. H.-K.C. and J.-T.H. wrote the paper. All authors read and approved the final manuscript.

ACKNOWLEDGEMENTS

This work was supported by the Main Research Program (E-0150301) of the Korea Food Research Institute (KFRI), funded by the Ministry of Science, ICT and Future Planning.

CONFLICT OF INTEREST STATEMENT

The authors have declared no conflicts of interest.

APPENDIX A. SUPPLEMENTARY DATA

Supplementary data to this article can be found online at <https://doi.org/10.1016/j.molmet.2018.11.001>.

REFERENCES

- [1] Ahmed, A., Wong, R.J., Harrison, S.A., 2015. Nonalcoholic fatty liver disease review: diagnosis, treatment, and outcomes. *Clinical Gastroenterology and Hepatology* 13(12):2062–2070.
- [2] Armstrong, M.J., Adams, L.A., Canbay, A., Syn, W.K., 2014. Extrahepatic complications of nonalcoholic fatty liver disease. *Hepatology* 59(3):1174–1197.

- [3] Byrne, C.D., Targher, G., 2015. NAFLD: a multisystem disease. *Journal of Hepatology* 62(Suppl. 1):S47–S64.
- [4] Tuomilehto, J., Lindstrom, J., Eriksson, J.G., Valle, T.T., Hamalainen, H., Ilanne-Parikka, P., et al., 2001. Prevention of type 2 diabetes mellitus by changes in lifestyle among subjects with impaired glucose tolerance. *New England Journal of Medicine* 344(18):1343–1350.
- [5] Bass, J., Takahashi, J.S., 2010. Circadian integration of metabolism and energetics. *Science* 330(6009):1349–1354.
- [6] Desvergne, B., Michalik, L., Wahli, W., 2006. Transcriptional regulation of metabolism. *Physiological Reviews* 86(2):465–514.
- [7] Lawless, M.W., Norris, S., O'Byrne, K.J., Gray, S.G., 2009. Targeting histone deacetylases for the treatment of immune, endocrine & metabolic disorders. *Endocrine Metabolic & Immune Disorders Drug Targets* 9(1):84–107.
- [8] Yan, W., Herman, J.G., Guo, M., 2016. Epigenome-based personalized medicine in human cancer. *Epigenomics* 8(1):119–133.
- [9] Alam, S., Mustafa, G., Alam, M., Ahmad, N., 2016. Insulin resistance in development and progression of nonalcoholic fatty liver disease. *World Journal of Gastrointestinal Pathophysiology* 7(2):211–217.
- [10] Buzzetti, E., Pinzani, M., Tsochatzis, E.A., 2016. The multiple-hit pathogenesis of non-alcoholic fatty liver disease (NAFLD). *Metabolism* 65(8):1038–1048.
- [11] Miao, F., Gonzalo, I.G., Lanting, L., Natarajan, R., 2004. In vivo chromatin remodeling events leading to inflammatory gene transcription under diabetic conditions. *Journal of Biological Chemistry* 279(17):18091–18097.
- [12] Xu, X., So, J.S., Park, J.G., Lee, A.H., 2013. Transcriptional control of hepatic lipid metabolism by SREBP and ChREBP. *Seminars in Liver Disease* 33(4):301–311.
- [13] Bricambert, J., Miranda, J., Benhamed, F., Girard, J., Postic, C., Dentin, R., 2010. Salt-inducible kinase 2 links transcriptional coactivator p300 phosphorylation to the prevention of ChREBP-dependent hepatic steatosis in mice. *Journal of Clinical Investigation* 120(12):4316–4331.
- [14] Martinek, R.G., Wolman, W., 1955. Xanthines, tannins, and sodium in coffee, tea, and cocoa. *Journal of the American Medical Association* 158(12):1031–1051.
- [15] Karakurt, S., Adali, O., 2016. Tannic acid inhibits proliferation, migration, invasion of prostate cancer and modulates drug metabolizing and antioxidant enzymes. *Anti Cancer Agents in Medicinal Chemistry* 16(6):781–789.
- [16] Tikoo, K., Sane, M.S., Gupta, C., 2011. Tannic acid ameliorates doxorubicin-induced cardiotoxicity and potentiates its anti-cancer activity: potential role of tannins in cancer chemotherapy. *Toxicology and Applied Pharmacology* 251(3):191–200.
- [17] Chen, X., Beutler, J.A., McCloud, T.G., Loehfelm, A., Yang, L., Dong, H.F., et al., 2003. Tannic acid is an inhibitor of CXCL12 (SDF-1alpha)/CXCR4 with antiangiogenic activity. *Clinical Cancer Research* 9(8):3115–3123.
- [18] Lei, F., Zhang, X.N., Wang, W., Xing, D.M., Xie, W.D., Su, H., et al., 2007. Evidence of anti-obesity effects of the pomegranate leaf extract in high-fat diet induced obese mice. *International Journal of Obesity (London)* 31(6):1023–1029.
- [19] Nie, F., Liang, Y., Xun, H., Sun, J., He, F., Ma, X., 2015. Inhibitory effects of tannic acid in the early stage of 3T3-L1 preadipocytes differentiation by down-regulating PPARgamma expression. *Food & Function* 6(3):894–901.
- [20] Kim, C.H., Younossi, Z.M., 2008. Nonalcoholic fatty liver disease: a manifestation of the metabolic syndrome. *Cleveland Clinic Journal of Medicine* 75(10):721–728.
- [21] Schmittgen, T.D., Livak, K.J., 2008. Analyzing real-time PCR data by the comparative C(T) method. *Nature Protocols* 3:1101–1108.
- [22] Choi, H.K., Choi, Y., Park, E.S., Park, S.Y., Lee, S.H., Seo, J., et al., 2015. Programmed cell death 5 mediates HDAC3 decay to promote genotoxic stress response. *Nature Communications* 6:7390.
- [23] Athar, M., Khan, W.A., Mukhtar, H., 1989. Effect of dietary tannic acid on epidermal, lung, and forestomach polycyclic aromatic hydrocarbon metabolism and tumorigenicity in Sencar mice. *Cancer Research* 49:5784–5788.
- [24] Peaslee, M.H., Einhellig, F.A., 1977. Protective effect of tannic acid in mice receiving dietary lead. *Experientia* 33:1206.
- [25] Lin, G.H., Xie, J.X., Cui, X.F., Nevo, E., Su, J.P., Zhang, T.Z., 2012. Effects of supplemental dietary tannic acid on digestion in Plateau Zokors (*Eospalax baileyi*). *Annales Zoologici Fennici* 49:371–377.
- [26] Sharma, R., Zhou, M.M., 2015. Partners in crime: the role of tandem modules in gene transcription. *Protein Science* 24:1347–1359.
- [27] Ferri, E., Petosa, C., McKenna, C.E., 2016. Bromodomains: structure, function and pharmacology of inhibition. *Biochemical Pharmacology* 106:1–18.
- [28] Delvecchio, M., Gaucher, J., Aguilar-Gurrieri, C., Ortega, E., Panne, D., 2013. Structure of the p300 catalytic core and implications for chromatin targeting and HAT regulation. *Nature Structural & Molecular Biology* 20:1040–1046.
- [29] Rack, J.G.M., Lutter, T., Kjaereng Bjerga, G.E., Guder, C., Ehrhardt, C., Varv, S., et al., 2014. The PHD finger of p300 influences its ability to acetylate histone and non-histone targets. *Journal of Molecular Biology* 426:3960–3972.
- [30] Wang, F., Marshall, C.B., Ikura, M., 2013. Transcriptional/epigenetic regulator CBP/p300 in tumorigenesis: structural and functional versatility in target recognition. *Cellular and Molecular Life Sciences* 70:3989–4008.
- [31] Remmert, M., Biegert, A., Hauser, A., Soding, J., 2011. HHblits: lightning-fast iterative protein sequence searching by HMM-HMM alignment. *Nature Methods* 9:173–175.
- [32] Humphrey, W., Dalke, A., Schulten, K., 1996. VMD: visual molecular dynamics. *Journal of Molecular Graphics* 14(33–38):27–38.
- [33] Wang, Y., Xiao, J., Suzek, T.O., Zhang, J., Wang, J., Bryant, S.H., 2009. PubChem: a public information system for analyzing bioactivities of small molecules. *Nucleic Acids Research* 37:W623–W633.
- [34] Trott, O., Olson, A.J., 2010. AutoDock Vina: improving the speed and accuracy of docking with a new scoring function, efficient optimization, and multi-threading. *Journal of Computational Chemistry* 31:455–461.
- [35] Choi, K.C., Jung, M.G., Lee, Y.H., Yoon, J.C., Kwon, S.H., Kang, H.B., et al., 2009. Epigallocatechin-3-gallate, a histone acetyltransferase inhibitor, inhibits EBV-induced B lymphocyte transformation via suppression of RelA acetylation. *Cancer Research* 69(2):583–592.
- [36] Mikula, M., Majewska, A., Ledwon, J.K., Dzwonek, A., Ostrowski, J., 2014. Obesity increases histone H3 lysine 9 and 18 acetylation at Tnfa and Ccl2 genes in mouse liver. *International Journal of Molecular Medicine* 34(6):1647–1654.
- [37] Zeybel, M., Mann, D.A., Mann, J., 2013. Epigenetic modifications as new targets for liver disease therapies. *Journal of Hepatology* 59(6):1349–1353.
- [38] Bowman, G.D., Poirier, M.G., 2015. Post-translational modifications of histones that influence nucleosome dynamics. *Chemical Reviews* 115(6):2274–2295.
- [39] Zhu, W.G., Otterson, G.A., 2003. The interaction of histone deacetylase inhibitors and DNA methyltransferase inhibitors in the treatment of human cancer cells. *Current Medicinal Chemistry Anti Cancer Agents* 3(3):187–199.
- [40] Wapenaar, H., Dekker, F.J., 2016. Histone acetyltransferases: challenges in targeting bi-substrate enzymes. *Clinical Epigenetics* 8:59.
- [41] Manzo, F., Tambaro, F.P., Mai, A., Altucci, L., 2009. Histone acetyltransferase inhibitors and preclinical studies. *Expert Opinion on Therapeutic Patents* 19(6):761–774.
- [42] Balasubramanyam, K., Altaf, M., Varier, R.A., Swaminathan, V., Ravindran, A., Sadhale, P.P., et al., 2004. Polyisoprenylated benzophenone, garcinol, a natural histone acetyltransferase inhibitor, represses chromatin transcription and alters global gene expression. *Journal of Biological Chemistry* 279(32):33716–33726.
- [43] Balasubramanyam, K., Varier, R.A., Altaf, M., Swaminathan, V., Siddappa, N.B., Ranga, U., et al., 2004. Curcumin, a novel p300/CREB-binding protein-specific inhibitor of acetyltransferase, represses the acetylation of histone/nonhistone proteins and histone acetyltransferase-dependent chromatin transcription. *Journal of Biological Chemistry* 279(49):51163–51171.

- [44] Sun, Y., Jiang, X., Chen, S., Price, B.D., 2006. Inhibition of histone acetyltransferase activity by anacardic acid sensitizes tumor cells to ionizing radiation. *FEBS Letters* 580(18):4353–4356.
- [45] Islam, M.A., Alam, F., Solayman, M., Khalil, M.I., Kamal, M.A., Gan, S.H., 2016. Dietary phytochemicals: natural swords combating inflammation and oxidation-mediated degenerative diseases. *Oxidative Medicine and Cellular Longevity* 2016, 5137431.
- [46] Zhao, S., Xu, W., Jiang, W., Yu, W., Lin, Y., Zhang, T., et al., 2010. Regulation of cellular metabolism by protein lysine acetylation. *Science* 327(5968):1000–1004.
- [47] Aagaard-Tillery, K.M., Grove, K., Bishop, J., Ke, X., Fu, Q., McKnight, R., et al., 2008. Developmental origins of disease and determinants of chromatin structure: maternal diet modifies the primate fetal epigenome. *Journal of Molecular Endocrinology* 41(2):91–102.
- [48] Liu, X., Kim, J.K., Li, Y., Li, J., Liu, F., Chen, X., 2005. Tannic acid stimulates glucose transport and inhibits adipocyte differentiation in 3T3-L1 cells. *Journal of Nutrition* 135(2):165–171.
- [49] Do, G.M., Kwon, E.Y., Ha, T.Y., Park, Y.B., Kim, H.J., Jeon, S.M., et al., 2011. Tannic acid is more effective than clofibrate for the elevation of hepatic beta-oxidation and the inhibition of 3-hydroxy-3-methyl-glutaryl-CoA reductase and aortic lesion formation in apo E-deficient mice. *British Journal of Nutrition* 106(12):1855–1863.
- [50] De Long, N.E., Hardy, D.B., Ma, N., Holloway, A.C., 2017. Increased incidence of non-alcoholic fatty liver disease in male rat offspring exposed to fluoxetine during fetal and neonatal life involves the NLRP3 inflammasome and augmented de novo hepatic lipogenesis. *Journal of Applied Toxicology* 37(12): 1507–1516.
- [51] de Moraes Maciel, R., de Silva Dutra, D.L., Rumjanek, F.D., Juliano, L., Juliano, M.A., Fantappie, M.R., 2004. Schistosoma mansoni histone acetyltransferase GCN5: linking histone acetylation to gene activation. *Molecular and Biochemical Parasitology* 133(1):131–135.
- [52] Chakravarti, D., LaMorte, V.J., Nelson, M.C., Nakajima, T., Schulman, I.G., Juguilon, H., et al., 1996. Role of CBP/P300 in nuclear receptor signalling. *Nature* 383(6595):99–103.
- [53] Giandomenico, V., Simonsson, M., Gronroos, E., Ericsson, J., 2003. Coactivator-dependent acetylation stabilizes members of the SREBP family of transcription factors. *Molecular and Cellular Biology* 23(7):2587–2599.
- [54] Gelman, L., Zhou, G., Fajas, L., Raspe, E., Fruchart, J.C., Auwerx, J., 1999. p300 interacts with the N- and C-terminal part of PPARgamma2 in a ligand-independent and -dependent manner, respectively. *Journal of Biological Chemistry* 274(12):7681–7688.
- [55] Tian, Y., Wong, V.W., Chan, H.L., Cheng, A.S., 2013. Epigenetic regulation of hepatocellular carcinoma in non-alcoholic fatty liver disease. *Seminars in Cancer Biology* 23(6 Pt B):471–482.
- [56] Chen, Q., Wang, T., Li, J., Wang, S., Qiu, F., Yu, H., et al., 2017. Effects of natural products on fructose-induced nonalcoholic fatty liver disease (NAFLD). *Nutrients* 9(2).
- [57] Yao, H., Qiao, Y.J., Zhao, Y.L., Tao, X.F., Xu, L.N., Yin, L.H., et al., 2016. Herbal medicines and nonalcoholic fatty liver disease. *World Journal of Gastroenterology* 22(30):6890–6905.
- [58] Ong, K.C., Khoo, H.E., Das, N.P., 1995. Tannic acid inhibits insulin-stimulated lipogenesis in rat adipose tissue and insulin receptor function in vitro. *Experientia* 51(6):577–584.
- [59] Zou, B., Ge, Z.Z., Zhang, Y., Du, J., Xu, Z., Li, C.M., 2014. Persimmon tannin accounts for hypolipidemic effects of persimmon through activating of AMPK and suppressing NF-kappaB activation and inflammatory responses in high-fat diet rats. *Food & Function* 5(7):1536–1546.
- [60] Gang, X., Yang, Y., Zhong, J., Jiang, K., Pan, Y., Karnes, R.J., et al., 2016. P300 acetyltransferase regulates fatty acid synthase expression, lipid metabolism and prostate cancer growth. *Oncotarget* 7(12):15135–15149.
- [61] Lee, J.H., Friso, S., Choi, S.W., 2014. Epigenetic mechanisms underlying the link between non-alcoholic fatty liver diseases and nutrition. *Nutrients* 6(8): 3303–3325.
- [62] Krautkramer, K.A., Kreznar, J.H., Romano, K.A., Vivas, E.I., Barrett-Wilt, G.A., Rabaglia, M.E., et al., 2016. Diet-microbiota interactions mediate global epigenetic programming in multiple host tissues. *Molecular Cell* 64(5):982–992.
- [63] Pham, T.X., Lee, J., 2012. Dietary regulation of histone acetylases and deacetylases for the prevention of metabolic diseases. *Nutrients* 4(12):1868–1886.
- [64] Marquardt, R.R., Ward, A.T., Campbell, L.D., Cansfield, P.E., 1977. Purification, identification and characterization of a growth inhibitor in faba beans (*Vicia faba* L. var. minor). *Journal of Nutrition* 107(7):1313–1324.
- [65] Featherston WR, R.J., 1975. Influence of tannins on the utilization of sorghum grain by rats and chicks. *Nutrition Reports International* 11:7.
- [66] Glick, Z., Joslyn, M.A., 1970. Effect of tannic acid and related compounds on the absorption and utilization of proteins in the rat. *Journal of Nutrition* 100(5): 516–520.
- [67] Manning, E.T., Ikehara, T., Ito, T., Kadonaga, J.T., Kraus, W.L., 2001. p300 forms a stable, template-committed complex with chromatin: role for the bromodomain. *Molecular and Cellular Biology* 21(12):3876–3887.
- [68] Nunez-Duran, H., 1980. Tannic acid as an electron microscope tracer for permeable cell membranes. *Stain Technology* 55(6):361–365.
- [69] Erdelyi, I., Levenkova, N., Lin, E.Y., Pinto, J.T., Lipkin, M., Quimby, F.W., et al., 2009. Western-style diets induce oxidative stress and dysregulate immune responses in the colon in a mouse model of sporadic colon cancer. *Journal of Nutrition* 139(11):2072–2078.
- [70] Itri, R., Junqueira, H.C., Mertins, O., Baptista, M.S., 2014. Membrane changes under oxidative stress: the impact of oxidized lipids. *Biophysical Reviews* 6(1): 47–61.
- [71] Asadi, E., Abdouss, M., Leblanc, R.M., Ezzati, N., Wilson, J.N., Azodi-Deilami, S., 2016. In vitro/in vivo study of novel anti-cancer biodegradable cross-linked tannic acid for fabrication of 5-fluorouracil-targeting drug delivery nano-device based on a molecular imprinted polymer. *RSC Advances* 6:11.